Origin of hysteresis between charge and discharge processes in lithium-rich layer-structured cathode material for lithium-ion battery

CrossMark

Hiroaki Konishi[*], Tatsumi Hirano, Daiko Takamatsu, Akira Gunji, Xiaoliang Feng, Sho Furutsuki

Hitachi Research Laboratory, Hitachi Ltd., 7-1-1 Omika-cho, Hitachi, Ibaraki 319-1292, Japan

HIGHLIGHTS

- There is large hysteresis between charge and discharge curves in $Li_{1.2}Ni_{0.13}Mn_{0.54}Co_{0.13}O_2$.
- Lattice parameter at the same SOC differs in charge and discharge processes.
- Oxidation state of each element at the same SOC differs in charge and discharge processes.

ARTICLE INFO

ABSTRACT

There is large hysteresis between charge and discharge curves in lithium-rich layer-structured cathode material, $Li_{1.2}Ni_{0.13}Mn_{0.54}Co_{0.13}O_2$. The mechanism for hysteresis was examined by X-ray diffraction (XRD) and X-ray absorption fine structure (XAFS) measurement as a first step in solving this issue. XRD measurements clarified that there was hysteresis in the lattice parameter between charge and discharge processes. XAFS spectra indicated that transition metals were oxidized and reduced in the same potential region during charge and discharge processes. Oxygen was oxidized at higher potential than transition metals during charge process; however, the former was reduced at lower potential than the latter during discharge process. Therefore, large hysteresis of potential between charge and discharge processes in $Li_{1.2}Ni_{0.13}Mn_{0.54}Co_{0.13}O_2$ was mainly related to the reaction which is compensated with redox of oxygen.

© 2015 Elsevier B.V. All rights reserved.

1. Introduction

High energy density has been required for lithium-ion batteries due to the development of electronic devices. Therefore, high levels of performance are required for electrode materials. Lithium-rich layer-structured cathode material, $Li[Li_{1-a-b-c}Ni_aMn_bM_c]O_2$ (M: metal), is a promising cathode material due to its high capacity with more than 200 Ah kg^{-1} [1–6]. However, this material has several drawbacks such as high-rate performance [7–9], cycling performance [7,10–12], and large hysteresis between charge and discharge curves [13–16]. Surface treatment and pre-cycling treatment effectively improve rate performance and cycling performance [7–12]. However, effective methods of improving hysteresis between charge and discharge curves have yet to be clarified. This problem causes a decline in energy efficiency during charge and discharge processes.

We tried to clarify the cause of large hysteresis in the present study as a first step toward solving this issue. Open circuit potential (OCP) during charge and discharge processes was measured. Furthermore, the change in lattice parameter and oxidation state of each transition metal at various state of charge (SOC) was evaluated by X-ray diffraction (XRD) and X-ray absorption fine structure (XAFS) analyses, and the relationship among reaction potential, lattice parameter, and oxidation state of each transition metal was investigated.

2. Experimental

$Li_{1.2}Ni_{0.13}Mn_{0.54}Co_{0.13}O_2$ was synthesized by reacting stoichiometric mixtures of $Li(CH_3COO)\cdot2H_2O$, $Ni(CH_3COO)_2\cdot4H_2O$, $Mn(CH_3COO)_2\cdot4H_2O$, and $Co(CH_3COO)_2\cdot4H_2O$. These raw materials were stirred in distilled water for 1 h, and then dried. The mixture was pre-heated at 500 °C for 12 h in air, and then heated at 850 °C for 12 h in air.

The composition of the synthesized sample was measured using inductively coupled plasma atomic emission spectroscopy (ICP-AES, PerkinElmer, OPTIMA-3300XL).

The crystal structure of the synthesized sample was evaluated by XRD (Rigaku, Rint-2200). The diffraction data were recorded at a 0.02° step width over a 2θ range from 10 to 90° using a Rigaku diffractometer with Cu Kα radiation ($\lambda = 1.54$ Å).

The electrochemical characteristic of the synthesized sample was measured with a three-electrode electrochemical cell containing an $Li_{1.2}Ni_{0.13}Mn_{0.54}Co_{0.13}O_2$ electrode as a cathode, lithium foil as an anode, and a reference. The electrode was composed of the $Li_{1.2}Ni_{0.13}Mn_{0.54}Co_{0.13}O_2$ sample, carbon, and binder (85: 10: 5 wt.%). The electrolyte was a 1 M $LiPF_6$ solution containing a mixture of ethylene carbonate (EC), ethylmethyl carbonate (EMC), and dimethyl carbonate (DMC) (1: 2: 2 vol%). The charge−discharge capacity of the synthesized sample was measured within a potential range of 2.5−4.6 V vs. Li/Li$^+$. The electrochemical cell was charged at 0.05C ($1C = 260$ A kg^{-1}) to 4.6 V, and then held at 4.6 V until the charge current became less than 0.005C. After that, the electrochemical cell was discharged at 0.05C to 2.5 V.

The open circuit potential (OCP) was defined as the potential 5 h after a charge−discharge process was stopped. The potential data were recorded every 10% SOC during charge and discharge processes.

The crystal structure of the synthesized sample during the second charge−discharge processes was evaluated by XRD. The cell was decomposed and the electrode was washed with DMC after the cell was charged and/or discharged. The diffraction data of every 20% SOC were recorded at a 0.02° step width over a 2θ range from 10 to 70° using Cu Kα radiation.

The oxidation state of each transition metal was investigated by XAFS at the BL-9C of the Photon Factory (PF) for High Energy Accelerator Research (KEK) in Japan. The samples for XAFS were prepared with the same procedure as that used to prepare the XRD samples. The oxidation state of each transition metal was mainly evaluated by X-ray absorption near-edge structure (XANES) analysis. The Ni, Co, and Mn K-edge XANES spectra of the prepared samples were measured in transmission mode by using an Si(111) double-crystal monochromator. The XANES spectra were compared with those of the reference samples such as lithium transition metal oxide and transition metal oxide.

3. Results and discussion

3.1. Characterization of $Li_{1.2}Ni_{0.13}Mn_{0.54}Co_{0.13}O_2$ powder

Table 1 lists the result of ICP-AES of $Li_{1.2}Ni_{0.13}Mn_{0.54}Co_{0.13}O_2$ powder. Table 1 indicates that the result of elemental analysis agreed well with the targeted composition. Fig. 1 shows the XRD

Table 1
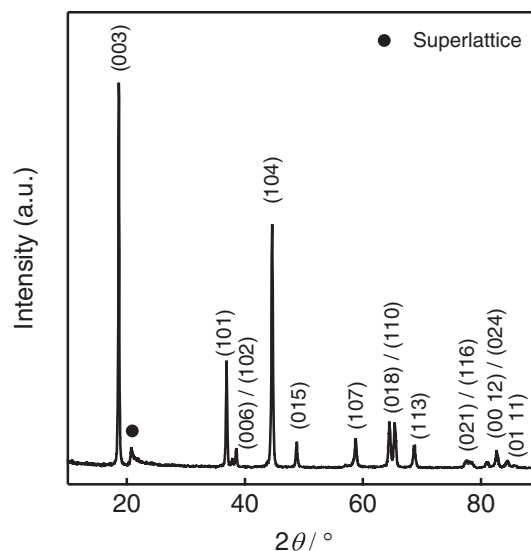Result of ICP-AES analysis of $Li_{1.2}Ni_{0.13}Mn_{0.54}Co_{0.13}O_2$ powder.

Composition			
Li	Ni	Mn	Co
1.22	0.13	0.54	0.13

Fig. 1. XRD pattern of $Li_{1.2}Ni_{0.13}Mn_{0.54}Co_{0.13}O_2$ powder.

pattern of $Li_{1.2}Ni_{0.13}Mn_{0.54}Co_{0.13}O_2$ powder. Every peak except for those between $2\theta = 20-25°$ could be assigned to the α-NaFeO$_2$ structure. The diffraction peaks between $2\theta = 20-25°$ were caused by superlattice ordering of lithium and transition metal in the transition metal layer [2,4–6].

3.2. Electrochemical properties of $Li_{1.2}Ni_{0.13}Mn_{0.54}Co_{0.13}O_2$

Fig. 2 shows the initial and second charge−discharge curves of $Li_{1.2}Ni_{0.13}Mn_{0.54}Co_{0.13}O_2$. The potential monotonically increased up to 4.4 V in the initial charge process, which corresponds to the oxidation of transition metal [3–5]. A plateau was observed above 4.4 V. The reaction in the plateau region is related to the irreversible oxygen loss from the lattice [1–6]. The potential monotonically decreased during the initial discharge process, and no plateau was observed. Therefore, there was large irreversible capacity and the hysteresis between the initial charge and discharge curves. This was attributed to the reaction in the plateau region. The Coulombic
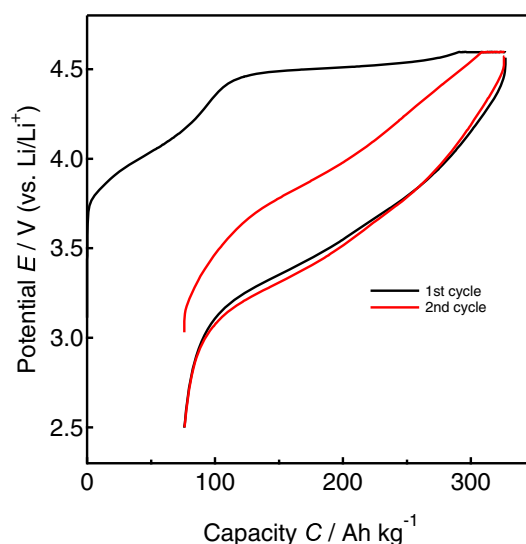

Fig. 2. Initial and second charge−discharge curves of $Li_{1.2}Ni_{0.13}Mn_{0.54}Co_{0.13}O_2$ within a potential range of 2.5−4.6 V vs. Li/Li$^+$.